Journal of Environmental Chemical Engineering 7 (2019) 102813

Contents lists available at ScienceDirect

Journal of Environmental Chemical Engineering

journal homepage: www.elsevier.com/locate/jece

Green Methanol Production Process from Indirect CO_2 Conversion: RWGS Reactor versus RWGS Membrane Reactor

Fereshteh Samimi, Nazanin Hamedi, Mohammad Reza Rahimpour*

Department of Chemical Engineering, Shiraz University, Shiraz, 71345, Iran

ARTICLE INFO

Keywords:
CO_2 Utilization
RWGS Reactor
H-SOD Membrane
Methanol Production
Process Modeling

ABSTRACT

Herein, two different scenarios for indirect CO_2 conversion process to produce methanol via reverse water gas shift (RWGS) reaction were investigated and compared. In the first scenario, CO_2 is converted to synthesis gas over $Fe_2O_3/Cr_2O_3/CuO$ catalyst in a RWGS reactor and then after passing a condenser to eliminate water, as an inhibitor of methanol synthesis catalyst, the product is sent to the methanol production reactor. While in the second, although the process is totally as the same as the previous one, a water permselective membrane was applied in the RWGS reactor. In this scenario, the produced water during the RWGS reaction is separated by the membrane; therefore, the free of water product no longer needed a separator before the methanol synthesis reactor. Both processes were numerically modeled and differential evolution (DE) method was employed to optimize the processes in order to achieve high methanol productivity. Also, the methanol production reactor from these two scenarios were compared with the conventional route (CR), in which methanol is produced from coal and natural gas. The results indicate that, in addition to water removal in the RWGS membrane reactor, a higher CO_2 conversion and CO yield and subsequently a more proper synthesis gas composition are obtained. More importantly, methanol production rate increases 13 ton/day (% 4.15 increase) and 109 ton/day (% 50.23 increase) in this scenario compared to the first scenario and CR. Also lower water is produced (17% reduction) in the methanol synthesis reactor of the second scenario respect to the first one.

1. Introduction

Global warming is currently one of the greatest threat to humanity and environment. CO2 accumulation in the atmosphere as a cause of fossil fuels combustion has a major contribution to global warming. CO2 capturing from large stationary emission sources and utilization as a feedstock for production of fuel products not only address the above problems, but also emerge as economically viable process [1–7]. Methanol (MeOH) is one of the candidate fuel products for the conversion of CO2 through a chemical process. As a raw material has a wide industrial applications for the production of methyl tertbutyl ether, dimethyl ether, dimethyl terephthalate, formaldehyde, methyl methacrylate, and acetic acid. Methanol can also be regarded as a vehicle fuel and as a fuel cell hydrogen carrier [8–10]. Hydrogen should be produced via a renewable energy (i.e., water splitting, solar, wind, geothermal, and biomass), in order to reduce the life cycle carbon dioxide emissions in the process. The eco-friendly sources of raw materials yields to an attractive green methanol synthesis process [11].

There are two different processes for methanol synthesis through CO2 chemical conversiondirect and indirect conversion of CO2. In the former, CO2 is directly converted into methanol, while in the later, CO2 is first converted into synthesis gas in a reverse water gas shift (RWGS) reactor, and then the produced synthesis gas is fed as the feedstock of methanol synthesis reactor [12]. Newly, Samimi et al. [13] have investigated methanol synthesis process from first route in three configurations with different cooling systems, namely water cooled, gas cooled and double cooled reactors. They presented and compared the capability of each configuration in converting CO2 to methanol by focusing on thermal behavior, possibility of second phase formation and effect of inlet pressure, inlet temperature and CO2/CO molar ratio.

The second route was first suggested by Joo et al. in 1999 [14]. After that some studies regarding to RWGS reaction were provided in the literature, when the focus of the researches was on the catalyst development and reaction mechanism. In 2001, Park et al. [15] synthesized and characterized ZnO/Al2O3 catalyst for the RWGS reaction. Cao et al. [16] investigated on Rh–Mo6S8 as the catalyst for the RWGS

Abbreviation: CR, Conventional route; DE, Differential evolution; H-SOD, Hydroxy sodalite; MeOH, Methanol; RWGS, Reverse water gas shift; RWGS-R, Reverse water gas shift reactor; RWGS-MR, Reverse water gas shift membrane reactor; SN, Stoichiometric number; WGS, Water gas shift

* Corresponding author.
E-mail address: rahimpor@shirazu.ac.ir (M.R. Rahimpour).

https://doi.org/10.1016/j.jece.2018.102813
Received 4 October 2018; Received in revised form 4 November 2018; Accepted 28 November 2018
Available online 29 November 2018
2213-3437/

Nomenclature

A_C	Cross sectional area (m2)
A_P	Perimeter area (m)
C_{pg}	Specific heat of the gas at constant pressure (J K^{-1} mol^{-1})
C_{pw}	Specific heat of water vapor in the reaction side (J K^{-1} mol^{-1})
d_p	Particle diameter (m)
F	Molar flow rate (mol s^{-1})
J_w	Water permeation rate (mol m^{-2} s^{-1})
h_f	Gas-solid heat transfer coefficient (W m^{-2} K^{-1})
h_i	Heat transfer coefficient between fluid phase and reactor wall in reaction side (W m^{-2} K^{-1})
h_o	Heat transfer coefficient between fluid phase and reactor wall in the permeation side (W m^{-2} K^{-1})
k_i	Rate constants for the ith reaction
K_i	Adsorption equilibrium constant
K_{pi}	Equilibrium constants
n	Fraction of feedstock to adjust syngas composition
P	Pressure (bar)
Q	Volumetric flow rate (m^3 s^{-1})
Q_w	H_2O permeance (mol s^{-1} m^{-2} Pa^{-1})
r_i	Rate of reaction of *i*th component (mol kg^{-1} s^{-1})
T	Temperature (K)
U	Overall heat transfer coefficient (W m^{-2} K^{-1})
y	Gas phase mole fraction
z	Variable represent length of reactor (m)

Greek letters

η	Effectiveness factor
ρ	Density of gas phase (kg m^{-3})
ρ_B	Bulk density (kg m^{-3})
ρ_p	Particle density (kg m^{-3})
μ	Viscosity of gas phase (kg m^{-1} s^{-1})
ϕ_s	Sphericity
ϕ_j	Thiele modulus
ε	Void fraction of catalyst bed
$\Delta H_{f,i}$	Enthalpy of formation of component *i* (J mol^{-1})

Subscripts

BW	Boiling water
perm	Permeation side
i	Chemical species
0	Inlet conditions
w	Water

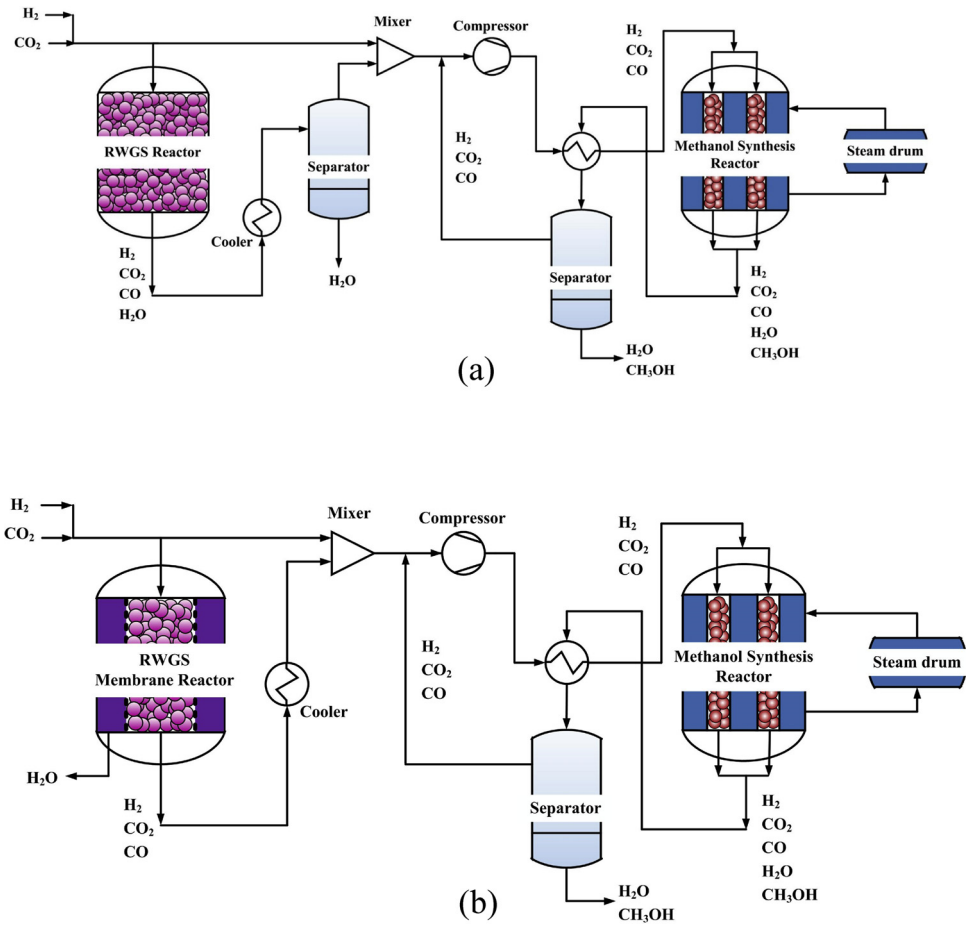

Fig. 1. A schematic diagram of the indirect CO_2 conversion process, (a) scenario 1 versus (b) scenario 2.

reaction. The mechanism and characteristics of the RWGS reaction was studied by Kim et al. [17] using Pt/TiO2 and Pt/Al2O3 catalysts. Their results indicated a higher turnover frequencies and CO2 conversion over Pt/TiO2. Chen and coworkers [18] synthesized silica-supported Cu nanoparticles for CO2 hydrogenation in RWGS reaction. It was observed that the reaction mechanism basically involves formate species formation. Anicic et al. [19] compared economical and energy-efficiency bases of direct and indirect conversion of CO2 in methanol production process. The results indicated that economically, the price of electricity had the most considerable impact as hydrogen is produced via the water electrolysis. Recently, Samimi et al. [20] have studied CO2 hydrogenation to methanol via RWGS reaction. In their work, the syngas was produced in a RWGS reactor over Ni/Al12O19 catalyst and then the syngas was sent to a methanol synthesis membrane reactor. They have applied a wo-dimensional model to evaluate both reactors performance.

In this work, Fe2O3/Cr2O3/CuO was applied as the catalyst of the RWGS reactor in indirect CO2 conversion process for methanol production. Two scenarios, where the difference between them is only in syngas production route, were modeled, optimized, and compared. In the first scenario, CO2 is converted into CO in the RWGS reactor, then the produced syngas passes a separator to eliminate water, while in the second scenario a water permselective membrane was coated the wall of RWGS reactor to eliminate water during the reaction. In the second process, there is no need to any separator for water removal from the syngas. A hydroxy sodalite (H-SOD) membrane was applied in this study for water separation. This membrane is a zeolite-like material with excellent selectivity of water. The ultimate value of water permeation through H-SOD was published 10-6 mol/(s m2 Pa) for an ideal case [21–23].

2. Process description

A schematic diagram of the indirect CO_2 conversion process for methanol production by two different scenarios was shown in Fig. 1(a,b).

2.1. The first scenario

The process consists of a RWGS reactor and a methanol synthesis reactor (see Fig. 1(a)). The feedstock which contains carbon dioxide and hydrogen are divided into two streams: the main is sent to the RWGS reactor, while the reminded part is required to adjust the composition of produced syngas. CO_2 and H_2 are partially converted to CO and H_2O by the RWGS reaction in an adiabatic reactor. The reaction products which include syngas (CO, CO_2 and H_2) and water are conveyed to a condenser to eliminate water from the stream, as it is a poison for the $Cu/ZnO/Al_2O_3$ catalyst in the next reactor. The produced syngas is then fed into the methanol synthesis reactor, after transmission through a series of compressors and a heat exchanger to attain the desired temperature and pressure of the reactor. Boiling water in the shell side of the reactor is used to control the temperature of exothermic reactions. Afterwards, the reactor outlet is transported to a condenser to separate methanol and water, as the condensable gases from the unreacted gas. Some part of the unreacted gas is recycled to the reactor to increase conversion.

Table 1
The operating conditions and reactor specifications of RWGS reactor.

Parameter	Values
Particle density (kg/m^3)	2628
Particle size (m)	$6 \times 6 \times 10^{-3}$
Length of reactor (m)	7
Diameter of reactor (m)	0.1292
Number of tubes	2962
Inlet pressure (bar)	1-30
Inlet temperature (°C)	100-450
Feed flow rate per tube (mol/s):	0.64
Feed composition (mole fraction):	
CO_2	0.25
H_2	0.75

2.2. The second scenario

In this scenario (see Fig. 1(b)), the process is totally as the same as the previous one, except that an H-SOD membrane for water removal was employed in the RWGS reactor, which can eliminate the intended separator after the reactor. As demonstrated in Fig. 2, the reactor walls were coated by the membrane. H_2O penetrates through the membrane layer during the reaction. A sweep gas (N_2) flows in the permeation side to carry the permeated H_2O.

The specifications and operating conditions of RWGS, RWGS membrane and methanol synthesis reactors were provided in Tables 1, 2 and 3 .

3. Reaction scheme and kinetics

3.1. RWGS reaction

For green methanol production process, RWGS reaction is needed for production of syngas. Because of high thermodynamic stability of CO_2, high amount of input energy (high temperature) is required for reaction with H_2 to produce CO and H_2O. However, temperature should be low as much as possible to minimize the capital costs and energy losses. CO_2 hydrogenation into CO and H_2O depends on the catalyst type, CO_2/H_2 ratio, and the reaction temperature and pressure. The RWGS is described as below:

$$CO_2 + H_2 \leftrightarrow CO + H_2O \; \Delta H^0_{298} = +41.2 kJ/mol_{CO_2} \quad (1)$$

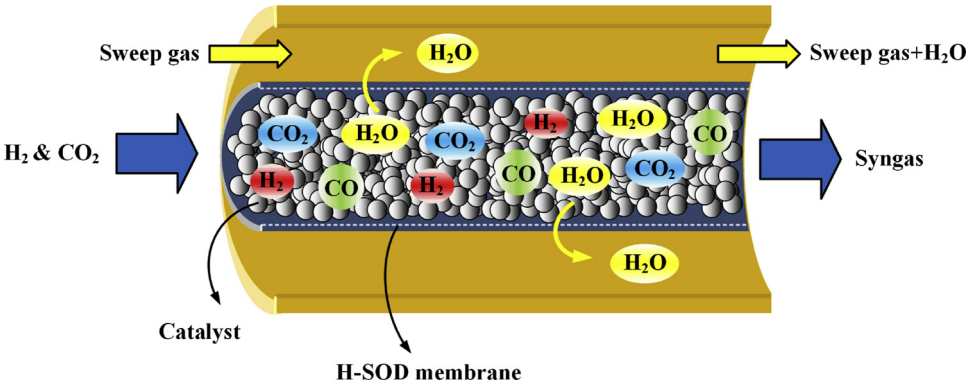

Fig. 2. A schematic of RWGS membrane reactor.

Table 2
The operating conditions and reactor specifications of RWGS membrane reactor.

Parameter	Values
Length of reactor (m)	7
Inner tube diameter (m)	0.1292
Outer tube diameter (m)	0.25
Number of tubes	2962
Sweep gas composition (mole fraction):	
H_2	0
H_2O	0
N_2	1
Sweep gas inlet temperature (°C)	27
Sweep gas inlet pressure (bar)	1
Sweep gas flow rate per tube (mol/s):	0.1

Table 3
The operating conditions and reactor specifications of methanol synthesis reactor.

Parameter	Values
Particle diameter (m)	5.47×10^{-3}
Bed void fraction	0.39
Density of catalyst bed (kg/m^3)	1140
Length of reactor (m)	7.022
Diameter of reactor (m)	3.8×10^{-2}
Number of tubes	2962
Inlet pressure (bar)	76.98
Inlet temperature (K)	503
Feed flow rate (mol/s)	0.64
Feed composition (mole fraction)[a,b]:	
CH_3OH	0.005
CO_2	0.094
CO	0.046
H_2O	0.0004
H_2	0.659
N_2	0.093
CH_4	0.1026

[a] *feed composition of conventional methanol synthesis reactor from natural gas.*
[b] *feed composition of methanol synthesis reactor in the indirect CO_2 conversion process is obtained in the present work after process modeling.*

$Fe_2O_3/Cr_2O_3/CuO$ as a well-known commercial catalyst for the water gas shift (WGS) reaction has been used in order to adjust the H_2/CO ratio in the syngas and thus it can be a logical candidate for the reverse reaction [12]. The kinetics of WGS reaction over this iron-based catalyst were developed by Hla et al. [24]. They determined the effects of CO, CO_2, H_2O and H_2 concentrations on the WGS reaction rate using four different inlet gas compositions and the catalyst was found to be more applicable to the gas streams with higher CO_2 levels. The reaction kinetic is described as below:

$$r = 10^{0.659\pm0.0125}\exp\left(\frac{-88 \pm 2.18}{R'T}\right)P_{CO}^{0.9\pm0.041}P_{H_2O}^{0.31\pm0.056}P_{CO_2}^{-0.156\pm0.078} P_{H_2}^{-0.05\pm0.006}(1-\beta) \quad (2)$$

$$\beta = \frac{1}{K}\left(\frac{P_{CO_2}P_{H_2}}{P_{CO}P_{H_2O}}\right) \quad (3)$$

where $R' = 8.314 \times 10^{-3}\left(\frac{kJ}{molK}\right)$ and K is the equilibrium constant of the reaction.

The above kinetic equation is derived at low pressures. Therefore, a pressure scale up correlation is required to apply a kinetic equation applicable at low pressures to higher pressures.

$$r = F_{press}\tilde{r} \quad (4)$$

where $\tilde{r}$ represents the reaction rate at atmospheric pressure and F_{press} indicates a pressure scale up factor. The following equation was proposed for high temperatures applications:

$$F_{press} = P^{0.5-P/250} \quad (5)$$

Where P is the actual reactor pressure in bar, valid up to 30 bar [25].

3.2. Methanol synthesis reactions

Methanol synthesis reactions are as below:

$$CO + 2H_2 \rightleftarrows CH_3OH\ \Delta H^0_{298} = -90.7kJ/mol_{CO} \quad (6)$$

$$CO_2 + H_2 \rightleftarrows CO + H_2O\ \Delta H^0_{298} = +41.2kJ/mol_{CO_2} \quad (7)$$

$$CO_2 + 3H_2 \rightleftarrows CH_3OH + H_2O\ \Delta H^0_{298} = -49.5kJ/mol_{CO_2} \quad (8)$$

The reactions kinetics of Graaf et al. [26] over $Cu/ZnO/Al_2O_3$ catalyst (as the commercial methanol synthesis catalyst) was selected. The reactions kinetics are expressed as below:

$$r_1 = \frac{k_1K_{CO}\left[f_{CO}f_{H_2}^{3/2} - \frac{f_{CH_2OH}}{f_{H_2}^{1/2}K^{p1}}\right]}{(1 + K_{CO}f_{CO} + K_{CO_2}f_{CO_2})\left[f_{H_2}^{1/2} + \left(\frac{K_{H_2O}}{K_{H_2}^{1/2}}\right)f_{H_2O}\right]} \quad (9)$$

$$r_2 = \frac{k_2K_{CO_2}\left[f_{CO_2}f_{H2} - \frac{f_{H_2O}f_{CO}}{K_{p2}}\right]}{(1 + K_{CO}f_{CO} + K_{CO_2}f_{CO_2})\left[f_{H_2}^{1/2} + \left(\frac{K_{H_2O}}{K_{H_2}^{1/2}}\right)f_{H_2O}\right]} \quad (10)$$

$$r_3 = \frac{k_3K_{CO_2}\left[f_{CO_2}f_{H_2}^{3/2} - \frac{f_{CH_3OH}f_{H_2O}}{f_{H_2}^{3/2}K_{p3}}\right]}{(1 + K_{CO}f_{CO} + K_{CO_2}f_{CO_2})\left[f_{H_2}^{1/2} + \left(\frac{K_{H_2O}}{K_{H_2}^{1/2}}\right)f_{H_2O}\right]} \quad (11)$$

f denotes as the fugacity of the component. The kinetic parameters were presented in Table 4.

For temperatures higher than 245 °C, which occurs in industrial methanol synthesis reactors, intra-particle diffusion limitations for the commercial catalyst pellet sizes should be taken into consideration. The dusty-gas model was employed by Lommerts et al. for considering internal mass transport limitations in methanol synthesis using pseudo first-order reaction rates for the formation of CH_3OH and H_2O as diffusion-limiting species [27]:

Table 4
The kinetic parameters of methanol synthesis reaction.

Rate constants [mol/s kg bar]		
$k = A\exp(\frac{B}{RT})$	A	B
k_1	$(4.89 \pm 0.29) \times 10^7$	$-63,000 \pm 300$
k_2	$(9.64 \pm 7.3) \times 10^{11}$	$-152,900 \pm 6800$
k_3	$(1.09 \pm 0.07) \times 10^5$	$-87,500 \pm 300$
Adsorption equilibrium constants		
$K = A\exp(\frac{B}{RT})$	A	B
K_{CO}	$(2.16 \pm 0.44) \times 10^{-5}$	$46,800 \pm 800$
$K_{CO}2$	$(7.05 \pm 1.39) \times 10^{-7}$	$61,700 \pm 800$
$\frac{K_{H_2O}}{K_{H_2}^{1/2}}$	$(6.37 \pm 2.88) \times 10^{-9}$	$84,000 \pm 1400$
Equilibrium constants		
$K_p = 10^{(\frac{A}{T-B})}$	A	B
K_{p1}	5139	12.621
K_{p2}	3066	10.592
K_{p3}	-2073	-2.029

$$r'_{CH_3OH} = k'_{CH_3OH}\left(C_{H_2} - \frac{C_{CH_3OH}}{K'^{eq}_{CH_3OH}}\right) \tag{12}$$

$$r'_{H_2O} = k'_{H_2O}\left(C_{H_2} - \frac{C_{H_2O}}{K'^{eq}_{H_2O}}\right) \tag{13}$$

where

$$K'^{ee}_{CH_3OH} = \frac{y^{eq}_{CH_3OH}}{y^{eq}_{H_2}} \tag{14}$$

$$K'^{eq}_{H_2O} = \frac{y^{eq}_{H_2O}}{y^{eq}_{H_2}} \tag{15}$$

The Thiele modulus is then described as:

$$\phi_j = \frac{d_p}{6}\sqrt{\frac{k'_j\rho_p(K'^{eq}_j + 1)}{D^{eff}_j K'^{eq}_j}} \tag{16}$$

$$\eta_j = \frac{1}{\phi_j}\left(\frac{1}{\tanh(3\phi_j)} - \frac{1}{3\phi_j}\right) \tag{17}$$

The effective diffusion coefficient, the Knudsen diffusion coefficient and the binary diffusion coefficient are estimated as follow:

$$\frac{1}{D^{eff}_{CH_3OH}} = \frac{\tau}{\varepsilon}\left(\frac{1}{D_{Knudsen,CH_3OH}} + \sum_{i\neq CH_3OH}^{N}\frac{y_i}{D_{CH_3OH,i}}\right) \tag{18}$$

$$\frac{1}{D^{eff}_{H_2O}} = \frac{\tau}{\varepsilon}\left(\frac{1}{D_{Knudsen,H_2O}} + \sum_{i\neq H_2O}^{N}\frac{y_i}{D_{H_2O,i}}\right) \tag{19}$$

$$D_{Knudsen,i} = \frac{d_{pore}}{3}\sqrt{\frac{8RT}{\pi MW_i}} \tag{20}$$

$$D_{i,j} = \frac{3.16\times10^{-8}T^{1.75}\left(\frac{1}{MW_i} + \frac{1}{MW_j}\right)^2}{P[(\sum v_i)^{1/3} + (\sum v_j)^{1/3}]^2} \tag{21}$$

τ is equal to 8.13, as the ratio between tortuosity and internal porosity of the catalyst pellet.

4. Mathematical model

4.1. RWGS membrane reactor

At first, a differential element with the length of dz in the axial direction was taken into consideration to obtain the governing equations. For a steady state, one dimensional homogeneous model, the material balance leads to ordinary differential equations:

Mass balances for H_2O in the reaction side:

$$-\frac{1}{A_{C1}}\frac{d}{dz}(F_{1i}) + \eta\rho_B r_i - (\frac{A_P}{A_{C1}})J_{H_2O} = 0 \tag{22}$$

i demonstrates the component numerator, F_{1i} is the component molar flow rate, A_{C1} is the cross sectional area, A_P is perimeter area and ρ_B is the catalyst bulk density.

Mass balances for H_2 in the reaction side:

$$-\frac{1}{A_{C1}}\frac{d}{dz}(F_{1i}) + \eta\rho_B r_i - 0.85(\frac{A_P}{A_{C1}})J_{H_2O} = 0 \tag{23}$$

Mass balances for other components in the reaction side:

$$-\frac{1}{A_{C1}}\frac{d}{dz}(F_{1i}) + \eta\rho_B r_i = 0 \tag{24}$$

where J_{H2O} is the water permeation in H-SOD membrane and is defined as below:

$$J_{H_2O} = Q_{H_2O}(P_{H_2O} - P^{perm}_{H_2O}) \tag{25}$$

It is worth mentioning that H-SOD membranes are not 100% selective to H_2O. Some amounts of hydrogen also permeate through the membrane. A H_2/H_2O selectivity equals to 0.85 at 389 °C was considered according to Rohde et al. [23]. Q_{H2O} is the H_2O permeance reported 10^{-7}–10^{-6} mol/(s m^2 Pa). In the present study, the value of 10^{-7} mol/(s m^2 Pa) was selected for the H_2O permeance.

Energy balances for the reaction side:

The RWGS reactor wall is supposed to be adiabatic; hence there is no heat transfer through the reactor wall.

$$\begin{aligned}&-\frac{C_{pg1}}{A_{C1}}\frac{d}{dz}(F_1T) + \rho_B\sum_{i=1}^{N}\eta r_i(-\Delta H_{f,i}) - U(\frac{A_P}{A_{C1}})(T - T_{perm})\\&- J_{H_2O}C_{p,H_2O}(\frac{A_P}{A_{C1}})(T - T_{ref})\\&-(0.85)J_{H_2O}C_{p,H_2}(\frac{A_P}{A_{C1}})(T - T_{ref}) = 0\end{aligned} \tag{26}$$

where T represents the temperature, C_{pg1} denotes the gas phase heat capacity, F_1 is the total molar flow rate and ΔH_{fi} demonstrates the heat change of the reaction.

Mass balance for H_2O in the permeation side:

$$-\frac{1}{A_{C1}}\frac{d}{dz}(F_{2i}) + \frac{A_P}{A_{C1}}J_{H_2O} = 0 \tag{27}$$

Mass balance for H_2 in the permeation side:

$$-\frac{1}{A_{C1}}\frac{d}{dz}(F_{2i}) + (0.85)\frac{A_P}{A_{C1}}J_{H_2O} = 0 \tag{28}$$

Mass balance for N_2 in the permeation side:

$$-\frac{d}{dz}(F_{2i}) = 0 \tag{29}$$

Energy balances for the permeation side:

$$\begin{aligned}&-\frac{C_{pg2}}{A_{C1}}\frac{d}{dz}(F_2T_{perm}) + U(\frac{A_P}{A_{C1}})(T - T_{perm}) + J_{H_2O}C_{p,H_2O}(T - T_{ref})\\&+(0.85)J_{H_2O}C_{p,H_2}(T - T_{ref}) = 0\end{aligned} \tag{30}$$

4.2. Methanol synthesis reactor

For a steady state, one dimensional homogeneous model, the following governing equations were derived.

Mass balances:

$$-\frac{1}{A_C}\frac{d}{dz}(F_i) + \eta\rho_B r_i = 0 \tag{31}$$

Energy balances:

$$-\frac{C_{pg}}{A_C}\frac{d}{dz}(FT) + \rho_B\sum_{i=1}^{N}\eta r_i(-\Delta H_{f,i}) - U_{shell}(\frac{A_p}{A_C})(T - T_{BW}) = 0 \tag{32}$$

Since the methanol synthesis reactor is surrounded by the boiling water to adsorb the generated heat, there is a heat transfer between the reaction and boiling water sides. T_{BW} is the boiling water temperature and U_{shell} is the overall heat transfer coefficient.

Ergun equation (pressure drop):

For estimation of pressure drop in both RWGS and methanol synthesis reactor, the following correlation is used.

$$\frac{dP}{dz} = 150\frac{\mu}{\varphi_s^2 d_p^2}\frac{(1-\varepsilon)^2}{\varepsilon^3}\frac{Q}{A_{c1}} + 1.75\frac{\rho}{\varphi_s d_p}\frac{(1-\varepsilon)}{\varepsilon^3}\frac{Q^2}{A_{c1}^2} \tag{33}$$

where Q and P refer to the volumetric flow rate and pressure, respectively; μ, ε, φ_s, d_p, A_c are the gas phase viscosity, bed porosity, catalyst sphericity, catalyst diameter and the reactor cross sectional area, respectively.

Boundary conditions:

$$z = 0:\ y_i = y_{i,0}\ T = T_0\ ,\ P = P_0 \tag{34}$$

Table 5
Auxiliary correlations in the mathematical modeling.

Parameter	Equation
Component heat capacity	$C_p = C_1 + C_2\left[\frac{C_3/T}{\sinh(C_3/T)}\right]^2 + C_4\left[\frac{C_5/T}{\sinh(C_5/T)}\right]^2$
Viscosity of reaction mixtures	$\mu = \frac{C_1 T^{C_2}}{1+\frac{C_3}{T}+\frac{C_4}{T^2}}$
Binary gas diffusion	$D_{ij} = \frac{10^{-7}T^{3/2}\sqrt{1/M_i + 1/M_j}}{P(v_{ci}^{3/2}+v_{cj}^{3/2})}$
Overall heat transfer coefficient	$\frac{1}{U} = \frac{1}{h_i +} + \frac{A_i \ln(D_o/D_i)}{2\pi L K_w} + \frac{A_i}{A_o}\frac{1}{h_o}$
Heat transfer coefficient between the gas phase and reactor wall	$\frac{h}{C_p \rho \mu}\left(\frac{C_p \mu}{K}\right)^{2/3} = \frac{0.458}{\varepsilon_B}\left(\frac{\rho u d_p}{\mu}\right)^{-0.407}$

The auxiliary correlations applied in the mathematical modeling were summarized in Table 5.

There are a set of ordinary differential equations which are coupled with algebraic equations consisting of ideal gas assumptions, reaction rates, heat and mass transfer coefficients correlations and physical properties of fluids. These equations form a set of non-linear algebraic equations using backward finite difference and solved by Gauss-Newton method in MATLAB programming environment.

4.3. Flash calculation

As noted, there are two separators in the indirect CO_2 conversion process which were also modeled. Flash calculation was used for separator model, in which the inlet temperature and pressure of the feed were known. The detail of the model and equations were provided in our previous work [28].

5. Optimization of the process

DE (Differential evolution) is a powerful, simple and fast method at numerical optimization and also is more likely to find a function's true global optimum [29,30]. There a lot of works in the literature in which DE strategy was employed to optimize a process through decision variables which may be the size of the equipment, the operating conditions or etc [31–38]. Babu and Angira provided the details of DE algorithm and pseudo code in their work [29]. The procedure applied in this work is "DE/best/1/bin" with NP (the number of population) equals to 30.

In this study, maximization of MeOH production rate in the both scenarios was considered as the objective function:

$$f = y_{MeOH} \tag{35}$$

Three decision variables namely, the inlet temperature (T_0) and pressure (P_0) of the RWGS reactor as well as the fraction of fresh feedstock (n) which is required to adjust the syngas composition were taken into consideration in both scenarios. The ranges of decision variables are:

$$100°C \le T_0 \le 450°C \tag{36}$$

$$1bar \le P_0 \le 30bar \tag{37}$$

$$0 < n < 1 \tag{38}$$

MeOH synthesis typically runs at 70-80 bar, and either the feed gas of RWGS reactor or the produced syngas needs to be compressed. RWGS reactor can operate up to 30 bar, thus the higher bound of 30 bar was considered for the pressure.

One constraint for the temperature bed of MeOH synthesis reactor was also considered in the optimization:

$$T < 550K \tag{39}$$

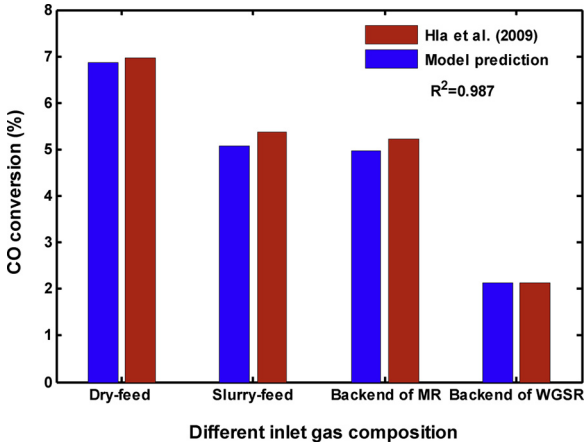

Fig. 3. A comparison between the RWGS reactor model and Hla et al. (2009) data. CO conversion during WGS reaction for dry-feed coal-derived syngas (65% CO, 30% H_2, 2% CO_2, 3% N_2), slurry-feed coal-derived syngas (44% CO, 37% H_2, 16% CO_2, 3% N_2), backend of catalytic membrane reactor (7% CO, 12% H_2, 78% CO_2, 3% N_2), backend of WGS reactor (4% CO, 55% H_2, 38% CO_2, 3% N_2).

The maximum temperature during the methanol synthesis reactions was selected to be lower than 550 K to be far away from catalyst deactivation ($Cu/ZnO/Al_2O_3$ catalyst cannot be used at temperatures above 573 K).

Penalty function procedure was then applied to add constraints into the optimization. In this work, 10^7 was chosen as the penalty parameter. The objective function finally was described as below:

Minimize:

$$F = -f + 10^7 G \tag{40}$$

where

$$G = \max\{0, (T - 550)\} \tag{41}$$

6. Model validation

There are two catalytic reactors in the indirect CO_2 conversion process: RWGS reactor and MeOH synthesis reactor. To prove the accuracy of the RWGS reactor model, the experimental work of Hla et al. [24] was simulated and the results were shown in Fig. 3. CO conversion during WGS reaction for four different inlet gas compositions (reacting temperature = 450 °C, 0.2 g of catalyst, wet gas velocity = 79.7 cm s^{-1} and steam: carbon ratio of 3) were compared. As shown the model predictions are in a reasonable agreement with the Kaiser et al. data. To verify the validity of the considered model in MeOH synthesis reactor, the simulation results of a conventional reactor were compared with the

Table 6
Comparison between model results and plant data of methanol synthesis reactor.

	Plant data		Model	Error %
	Reactor inlet	Reactor outlet	Reactor outlet	
Feed flow rate (mol s^{-1})	0.565	0.51	0.5065	-0.68
Temperature (K)	503	528	523.08	-0.93
Composition (mol%):				
CO_2	3.45	2.18	2.17	-0.45
H_2	79.55	75.71	75.51	-0.26
CO	4.66	1.44	1.09	-24.30
H_2O	0.08	1.74	1.76	1.14
CH_3OH	0.032	5.49	5.81	5.82
CH_4	11.72	12.98	13.07	0.69

plant data of Shiraz Petrochemical Company under the same process conditions. As listed in Table 6, there are a good agreement between the model and the plant data.

7. Results and discussion

7.1. The effect of inlet temperature and pressure on the performance of RWGS reactor and RWGS membrane reactor

It is noteworthy to mention that H_2O concentration and stoichiometric number (SN) of the produced syngas as a raw material for methanol synthesis reactor are the two important parameters need to be considered. The SN is defined as below:

$$SN = \frac{y_{H_2} - y_{CO_2}}{y_{CO} + y_{CO_2}} \quad (42)$$

The SN equal to 2 in a process including H_2, CO and CO_2 in the feedstock is desired. In the RWGS reactor, where CO_2 and H_2 are present in the feed gas, $H_2/CO_2 = 3$, results in SN = 2. Also, H_2O concentration in the feedstock of methanol synthesis reactor must not be higher than 1% vol, as its poisoning effect on the traditional methanol catalyst. For this purpose, in the first scenario, the produced water through the RWGS reactor is eliminated by a separator and then the syngas is sent to the methanol synthesis reactor, while in the second, this is done by applying a water permselective membrane in the reactor.

Fig. 4 shows the CO_2 conversion as a function of RWGS reactor (in the absence of membrane) inlet temperature and pressure in H_2/CO_2 inlet ratio equals to 3. A close look reveals that at temperatures lower than 500 K in all pressure ranges, CO_2 conversion is equal to zero, which means RWGS reaction requires a temperature higher than 500 K to begin. After that, CO_2 conversion increases with increasing reactor inlet temperature. This is because in high temperatures, the thermodynamic equilibrium shifts the RWGS reaction towards CO production. The effect of pressure is much lower than temperature, however the effect of pressure in the range of 1-10 bar is more pronounced for CO_2 conversion. The inlet pressure higher than 10 bar has no remarkable influence on the reactor performance.

The effect of inlet temperature and pressure of RWGS membrane reactor was also investigated in Fig. 5. In part (a), CO_2 conversion was demonstrated. In contrast to the previous case, the conversion of CO_2 is strongly dependent on the inlet pressure and it increases as the pressure increases. This is because in the reactor, a water permselective membrane was employed to separate water from the reaction side. By increasing the pressure differences between the reaction and permeation sides, the driving force for water separation also increases (the permeation side is operated at 1 bar). Therefore, by removing water from the reaction side (see part (b)), the RWGS reaction (reaction (1)) is shifted toward more CO production (see part (c)), and subsequently more CO_2 is consumed (part (a)).

As demonstrated, for a certain feed flow rate and H_2/CO_2 ratio, the CO_2 conversion and consequently the yield of CO is proportional to temperature and pressure of the feed stream for both scenarios. It means that it is possible to gain a composition of the produced syngas compatible with the methanol production process requirements by changing only the operating conditions of the RWGS reactor.

7.2. The effect of RWGS reactor inlet temperature on the performance of methanol synthesis reactor

Methanol production is a strongly function of CO content in the feedstock (just taking a close look at the reaction network). Thus, it is expected that more CO content in the feed gas results in a higher methanol yield. On the other hand, the amount of CO content in the feedstock (syngas) directly depends on the RWGS reactor conditions; mainly on the temperature. Therefore, it is clear that RWGS reactor temperature influences directly on the amount of methanol production rate. So in this section the effect of inlet temperature of the RWGS reactor (in the absence of membrane) was verified on the performance of methanol synthesis reactor.

Figs. 6(a-e) depict the changes in the mole fractions of different components versus temperature of the RWGS reactor and the length of methanol synthesis reactor. As seen in part (a), methanol as the main product is produced during the reactions and its concentration increases with augmentation of the RWGS reactor inlet temperature. Methanol increasing trend is more pronounced in higher temperatures (> 500 K), because of significantly high amount of CO in the feedstock at these temperatures. An inverse trend is observed for H_2O concentration (see part (b)). This is due to the fact that in the presence of high amount of CO in the feedstock (proportional to high RWGS reactor inlet temperature), the RWGS reaction (Eq. (7)) in the methanol synthesis reactor is shifted toward the left side (known as WGS reaction), and therefore the formation of water is reduced.

CO mole fraction distribution along the reactor was illustrated in part (c). At low temperatures of the RWGS reactor, CO is produced along the methanol reactor. When CO concentration is low in the feedstock, it is produced by the RWGS reaction (Eq. (7)) and the methanol is formed by CO_2 hydrogenation through reaction (8). As the amount of CO increases in the feedstock (with increasing the inlet temperature of the RWGS reactor), its generation rate is decreased and consumed by the WGS reaction (the reverse of Eq. (7)) and its hydrogenation to methanol (Eq. (6)). Almost an inverse trend occurs for CO_2 mole fraction (part (d)). At low temperatures of the RWGS reactor, the CO content in the produced syngas is very low, consequently CO_2 plays the main source of methanol production (Eq. (8)) and the RWGS reaction (Eq. (7)). Thus at low temperatures, CO_2 concentration in the feed stream is remarkably high and it is consumed during the reactor. With increasing the temperature, CO_2 concentration in the feedstock is reduced and consequently CO_2 is generated during the reactor as the results of the WGS reaction.

The changes of H_2 mole fraction were also investigated. Fig. 6(e) shows reduction of hydrogen along the reactor, due to CO and CO_2 hydrogenation to methanol. However, H_2 conversion is much more in high temperatures due to high CO concentration in the feedstock favors CO hydrogenation reaction and subsequently consuming more H_2. Also the initial concentration of H_2 in lower temperatures is much higher, because of lower H_2 conversion in the RWGS reactor in the lower temperatures.

Fig. 7 shows temperature profile along the methanol synthesis reactor as a function of the RWGS reactor temperature. As shown, there is a peak in the temperature profile at the first part of the methanol synthesis reactor due to exothermic nature of the reactions. However, by passing the fluid through the reactor, the effect of boiling water becomes more pronounced, and finally it overcomes the generated heat; and therefore the temperature is reduced. This figure also reveals that

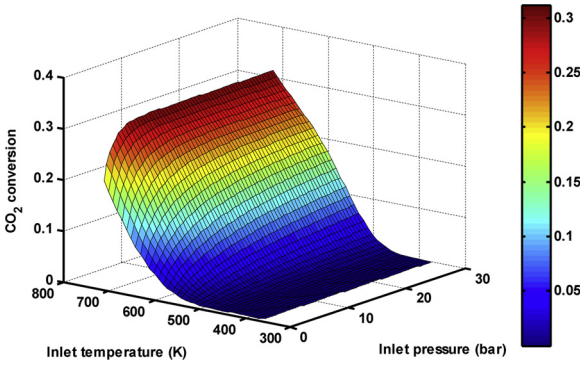

Fig. 4. CO_2 conversion as a function of inlet temperature and pressure of RWGS reactor.

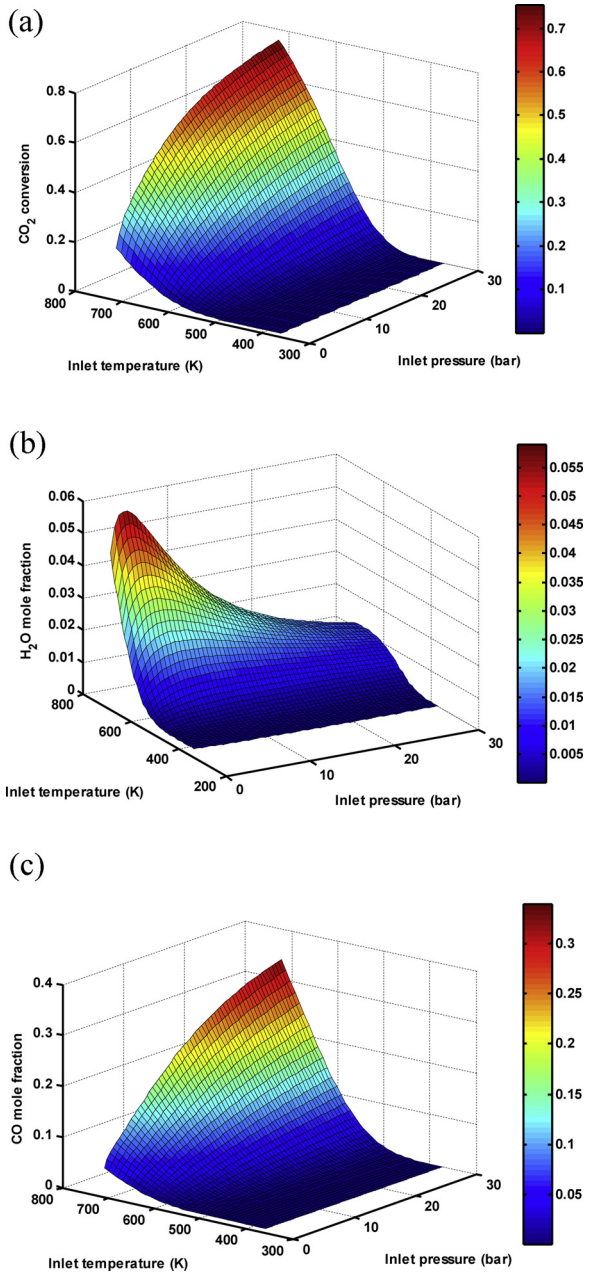

Fig. 5. (a) CO_2 conversion, (b) H_2O and (C) CO mole fractions of RWGS membrane reactor a function of inlet temperature and pressure.

that a rise in the RWGS reactor temperature (proportional to CO content) results to a higher hot spot in the reactor. This is because, increasing the CO content in the feedstock favors the exothermic WGS reaction, leads to more heat generation. Also, augmentation of CO concentration enhances the reaction rate; and subsequently, more heat is generated. Thus higher concentration of CO in the syngas shifts the equilibrium towards the exothermic reactions and makes controlling of the reactor thermal behavior more difficult.

Although methanol production favors in high RWGS reactor temperature (because of high CO content in the syngas feedstock), the temperature must be kept in the least possible way to minimize the capital costs and energy losses. Also higher temperatures of the RWGS reactor lead to a higher temperature in the methanol reactor bed, contributing to catalyst sintering. Therefore, it is essential to optimize the temperature and pressure of the RWGS reactor in order to keep it as low as possible and to gain a high methanol yield with a reasonable hot

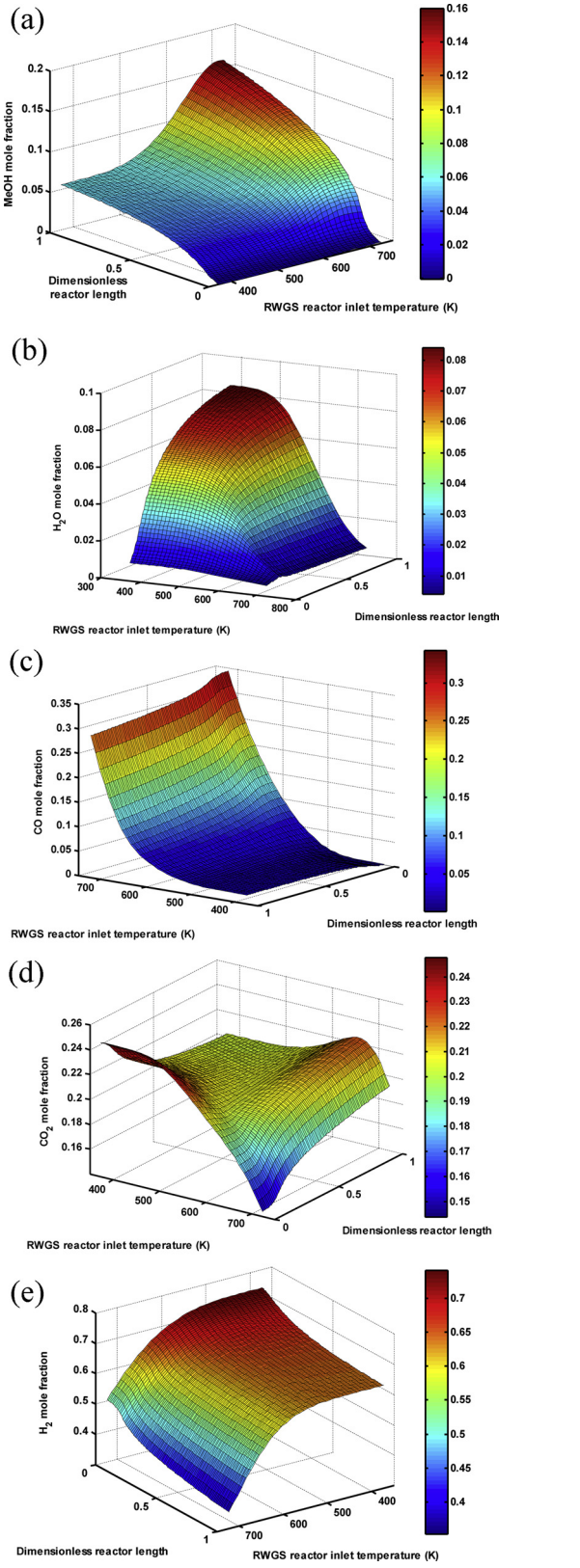

Fig. 6. The effect of inlet temperature of RWGS reactor (in the absence of membrane) on the mole fractions of different components of methanol synthesis reactor (a) MeOH mole fraction, (b) H_2O mole fraction, (c) CO mole fraction, (d) CO_2 mole fraction and (e) H_2 mole fraction.

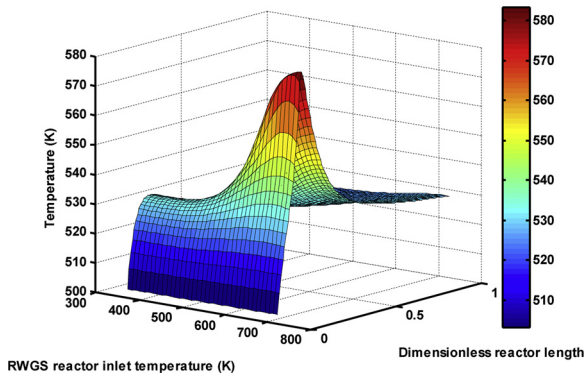

Fig. 7. The effect of RWGS reactor inlet temperature on the temperature profile of methanol synthesis reactor.

Table 7
Optimization results of both scenarios.

Decision variables	Scenario 1	Scenario 2
n_{RWGS}	0.76	0.5
Inlet temperature (°C)	450	389
Inlet pressure (bar)	23	30

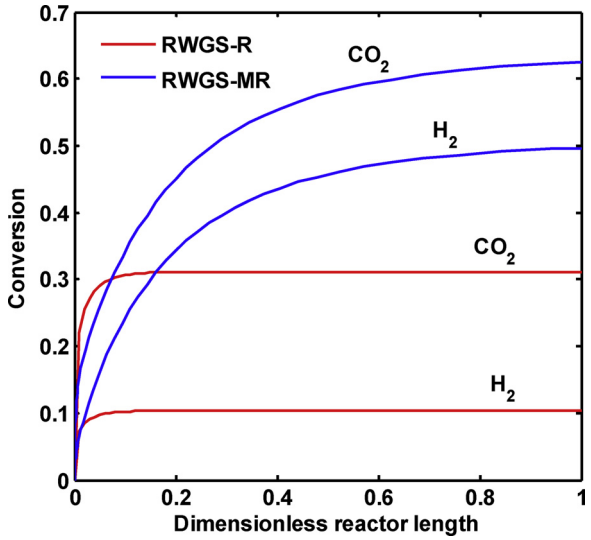

Fig. 8. A comparison between CO_2 and H_2 conversions along RWGS-R and RWGS-MR.

spot along the reactor. In the next section, the optimization results will be presented.

7.3. Optimization results

As mentioned, to gain high methanol productivity and a reasonable temperature profile along the methanol synthesis reactor, an optimization was performed to find the best values for the fraction of fresh feed as well as the RWGS reactor inlet temperature and pressure. Table 7 presents the results of optimization for both scenarios. In the next section, the numerical results of the process at the optimal conditions were presented.

7.3.1. RWGS reactor (RWGS-R) versus RWGS membrane reactor (RWGS-MR)

Fig. 8 displays CO_2 and H_2 conversions along both RWGS-R and RWGS-MR at the optimized conditions. CO_2 and H_2 as the reactants are consumed to produce CO and H_2O during the reactions. In RWGS-R, the

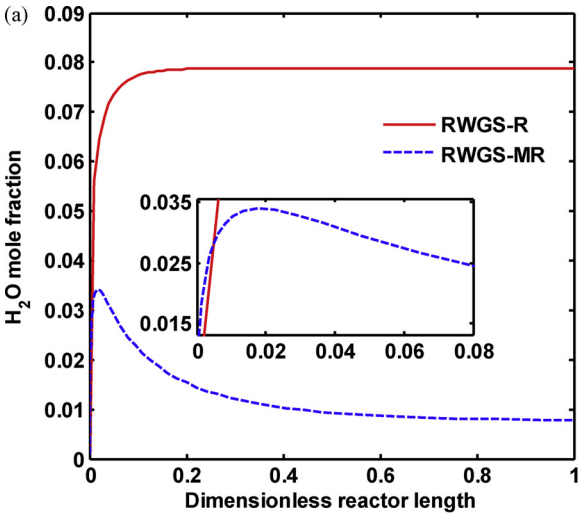

Fig. 9. A comparison of (a) H_2O mole fraction and (b) CO mole fraction along RWGS-R and RWGS-MR.

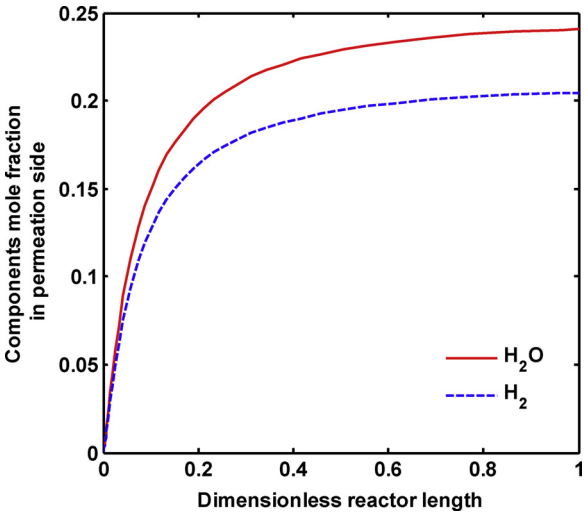

Fig. 10. H_2 and H_2O mole fractions in permeation side of RWGS-MR.

conversions of CO_2 and H_2 are increased along the reactor length and after reaching to the equilibrium follow a constant trend. While in the RWGS-MR, by removing water during the reaction, thermodynamic

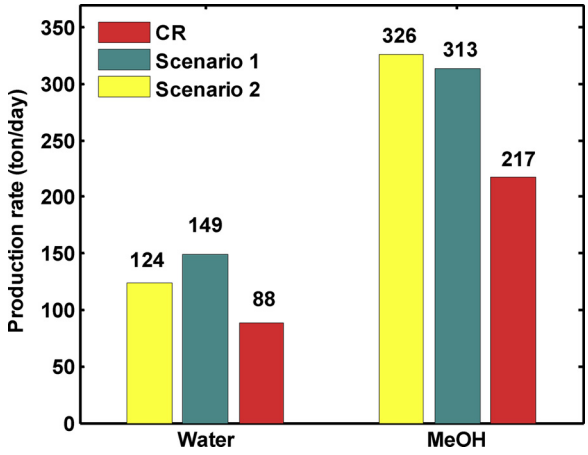

Fig. 11. A comparison between the performance of CR, scenario 1 and scenario 2 in MeOH and water production rate.

equilibrium is shifted toward more CO_2 and H_2 consumption and thus the higher conversions are achieved compared to the RWGS-R.

The products mole fractions at the optimized conditions were depicted in Fig. 9. H_2O mole fraction in the RWGS-R is increased and then follows a monotonous profile, while in the RWGS-MR, it first rises up to a certain point at the beginning of the reactor (because of the RWGS reaction) and then it diminishes along the rest of the reactor. This is due to the fact that from the peak point to the end of the reactor, water permeation rate through the membrane is higher than water production rate of the RWGS reaction, thus it is reduced. On the other hand, as illustrated in part (b), more CO is produced during water penetration through the membrane based on the Le Chatelier's principle (see Eq. (1)).

Fig. 10 shows H_2O and H_2 mole fractions distributions in the permeation side of the RWGS-MR. As before said, in addition to H_2O, some amounts of H_2 also diffuses through the H-SOD membrane at 389 °C. This is due to the fact that H_2O and H_2 kinetic diameters at this temperature (0.265 nm and 0.29, respectively) are smaller than the pore diameters of the zeolites; both molecules are separated. The permeation of H_2O in the zeolite diminishes with increasing temperature, and H_2O/H_2 permselectivity remarkably drops at high temperatures. H_2O permeance is between 1×10^{-7} and 10^{-6} mol/(s m^2 Pa) in the zeolite membranes. At 389 °C, a H_2/H_2O selectivity equals to 0.85 was taken into account based on the Rohde et al. work [23]. Therefore, H_2O and H_2 concentrations are increased in the permeation side during the reactor length and a lower concentration for H_2 is also observed.

7.3.2. A comparison among scenario 1, scenario 2 and the conventional route (CR)

Indirect CO_2 conversion process is a green methanol production route, since the feedstock contains CO_2 and renewable H_2. Two different scenarios were investigated in this research: scenario 1 and scenario 2. In the first, a RWGS reactor was applied to produce syngas, while in the second, a water permselective membrane was employed in the RWGS reactor. Here scenario 1 and 2 as two proposed routes of indirect CO_2 conversion process were compared with the conventional route (CR) of methanol synthesis from natural gas with the same operating conditions. Fig. 11 compares methanol and water production rates for CR and scenario 1 and scenario 2. Methanol is produced 217, 313 and 326 ton/day, while water production rate is 88, 149 and 124 ton/day in CR, scenario 1 and scenario 2, respectively. Scenario 2 produces 109 ton of methanol per day more than CR (50.23 % increase in methanol production rate), which is a considerable amount. In comparison with scenario 1, a lower water production is also formed in scenario 2 (17% reduction). These contribute to the fact that a higher CO concentration in the produced syngas for scenario 2 is achieved.

8. Conclusions

In the present work, the indirect CO_2 hydrogenation process for green methanol production in an industrial scale was numerically investigated and optimized via two different routes. In the first route (scenario 1), the produced syngas in a RWGS reactor passes a separator to remove water as the catalyst poisoning of methanol synthesis reactor. While in the second route (scenario 2), a water permselective membrane was applied in the RWGS reactor to separate water during the reaction and eliminate the intended separator in the process. Also the plausibility of these two scenarios to produce methanol was compared with the conventional methanol synthesis route (CR). The results indicated the superiority of scenario 2 to scenario 1, due to the following reasons:

- A higher CO_2 conversion and CO yield were achieved in scenario 2.
- A more suitable synthesis gas composition was gained in scenario 2.
- There is no need for further removal of water from syngas in separator in scenario 2.
- Methanol production was increased 13 ton/day (% 4.15 increase) in scenario 2 compared to scenario 1.
- Water production was reduced 17% in scenario 2 compared to scenario 1.

Also in comparison with CR, methanol production was increased 109 ton/day (% 50.23 increase) in scenario 2. Although the work is theoretical in nature, does show strongly the feasibility of the proposed process. However the costs of the respective implementation will need to be addressed in future work.

References

[1] A. Ateka, P. Pérez-Uriarte, M. Gamero, J. Ereña, A.T. Aguayo, J. Bilbao, A comparative thermodynamic study on the CO2 conversion in the synthesis of methanol and of DME, Energy 120 (2017) 796–804.
[2] N.v.d. Assen, L.J. Müller, A. Steingrube, P. Voll, A. Bardow, Selecting CO2 sources for CO2 utilization by environmental-merit-order curves, Environmental science & technology 50 (3) (2016) 1093–1101.
[3] A. Rafiee, K.R. Khalilpour, D. Milani, M. Panahi, Trends in CO2 conversion and utilization: A review from process systems Perspective, Journal of Environmental Chemical Engineering (2018).
[4] P. Kumar, P. With, V.C. Srivastava, R. Glaeser, I.M. Mishra, Conversion of carbon dioxide along with methanol to dimethyl carbonate over ceria catalyst, Journal of Environmental Chemical Engineering 3 (4) (2015) 2943–2947.
[5] W. Wisaijorn, Y. Poo-arporn, P. Marin, S. Ordóñez, S. Assabumrungrat, P. Praserthdam, D. Saebea, S. Soisuwan, Reduction of carbon dioxide via catalytic hydrogenation over copper-based catalysts modified by oyster shell-derived calcium oxide, Journal of Environmental Chemical Engineering 5 (4) (2017) 3115–3121.
[6] P. Akhter, M.A. Farkhondehfal, S. Hernández, M. Hussain, A. Fina, G. Saracco, A.U. Khan, N. Russo, Environmental issues regarding CO2 and recent strategies for alternative fuels through photocatalytic reduction with titania-based materials, Journal of Environmental Chemical Engineering 4 (4) (2016) 3934–3953.
[7] A. Ranjbar, A. Irankhah, S.F. Aghamiri, Reverse water gas shift reaction and CO2 mitigation: nanocrystalline MgO as a support for nickel based catalysts, Journal of Environmental Chemical Engineering 6 (4) (2018) 4945–4952.
[8] F. Samimi, M.R. Rahimpour, Direct Methanol Fuel Cell, Methanol, Elsevier, 2017, pp. 381–397.
[9] O.Y. Abdelaziz, W.M. Hosny, M.A. Gadalla, F.H. Ashour, I.A. Ashour, C.P. Hulteberg, Novel process technologies for conversion of carbon dioxide from industrial flue gas streams into methanol, Journal of CO2 Utilization 21 (2017) 52–63.
[10] N. Meiri, R. Radus, M. Herskowitz, Simulation of novel process of CO2 conversion to liquid fuels, Journal of CO2 Utilization 17 (2017) 284–289.
[11] S.G. Jadhav, P.D. Vaidya, B.M. Bhanage, J.B. Joshi, Catalytic carbon dioxide hydrogenation to methanol: a review of recent studies, Chemical Engineering Research and Design 92 (11) (2014) 2557–2567.
[12] M. De Falco, S. Giansante, G. Iaquaniello, L. Barbato, Methanol Production from CO 2 Via Reverse-Water–Gas-Shift Reaction, CO2: A Valuable Source of Carbon, Springer, 2013, pp. 171–186.
[13] F. Samimi, M. Feilizadeh, M. Ranjbaran, M. Arjmand, M.R. Rahimpour, Phase stability analysis on green methanol synthesis process from CO2 hydrogenation in water cooled, gas cooled and double cooled tubular reactors, Fuel Processing Technology 181 (2018) 375–387.
[14] O.-S. Joo, K.-D. Jung, I. Moon, A.Y. Rozovskii, G.I. Lin, S.-H. Han, S.-J. Uhm, Carbon dioxide hydrogenation to form methanol via a reverse-water-gas-shift reaction (the

CAMERE process), Industrial & engineering chemistry research 38 (5) (1999) 1808–1812.
[15] S.-W. Park, O.-S. Joo, K.-D. Jung, H. Kim, S.-H. Han, Development of ZnO/Al2O3 catalyst for reverse-water-gas-shift reaction of CAMERE (carbon dioxide hydrogenation to form methanol via a reverse-water-gas-shift reaction) process, Applied Catalysis A: General 211 (1) (2001) 81–90.
[16] Z. Cao, L. Guo, N. Liu, X. Zheng, W. Li, Y. Shi, J. Guo, Y. Xi, Theoretical study on the reaction mechanism of reverse water–gas shift reaction using a Rh–Mo 6 S 8 cluster, RSC Advances 6 (110) (2016) 108270–108279.
[17] S.S. Kim, H.H. Lee, S.C. Hong, A study on the effect of support's reducibility on the reverse water-gas shift reaction over Pt catalysts, Applied Catalysis A: General 423 (2012) 100–107.
[18] C.S. Chen, J.H. Wu, T.W. Lai, Carbon dioxide hydrogenation on Cu nanoparticles, The Journal of Physical Chemistry C 114 (35) (2010) 15021–15028.
[19] B. Anicic, P. Trop, D. Goricanec, Comparison between two methods of methanol production from carbon dioxide, Energy 77 (2014) 279–289.
[20] F. Samimi, D. Karimipourfard, M.R. Rahimpour, Green methanol synthesis process from carbon dioxide via reverse water gas shift reaction in a membrane reactor, Chemical Engineering Research and Design (2018).
[21] G. Bercic, J. Levec, Intrinsic and global reaction rate of methanol dehydration over, gamma.-alumina pellets, Industrial & engineering chemistry research 31 (4) (1992) 1035–1040.
[22] S. Khajavi, J.C. Jansen, F. Kapteijn, Application of a sodalite membrane reactor in esterification—Coupling reaction and separation, Catalysis Today 156 (3-4) (2010) 132–139.
[23] M. Rohde, G. Schaub, S. Khajavi, J. Jansen, F. Kapteijn, Fischer–Tropsch synthesis with in situ H2O removal–Directions of membrane development, Microporous and Mesoporous Materials 115 (1-2) (2008) 123–136.
[24] H.S.A.N. SHWE, D. Park, G. DUFFY, J. EDWARDS, D. ROBERTS, A. ILYUSHECHKIN, L. MORPETH, T. Nguyen, Kinetics of high-temperature water-gas shift reaction over two iron-based commercial catalysts using simulated coal-derived syngases, Chemical engineering journal 146 (1) (2009) 148–154.
[25] C. Singh, D.N. Saraf, Simulation of high-temperature water-gas shift reactors, Industrial & Engineering Chemistry Process Design and Development 16 (3) (1977) 313–319.
[26] G. Graaf, E. Stamhuis, A. Beenackers, Kinetics of low-pressure methanol synthesis, Chemical Engineering Science 43 (12) (1988) 3185–3195.
[27] B. Lommerts, G. Graaf, A. Beenackers, Mathematical modeling of internal mass transport limitations in methanol synthesis, Chemical Engineering Science 55 (23) (2000) 5589–5598.
[28] F. Samimi, M.R. Rahimpour, A. Shariati, Development of an Efficient Methanol Production Process for Direct CO2 Hydrogenation over a Cu/ZnO/Al2O3 Catalyst, Catalysts 7 (11) (2017) 332.
[29] B. Babu, R. Angira, Modified differential evolution (MDE) for optimization of non-linear chemical processes, Computers & chemical engineering 30 (6-7) (2006) 989–1002.
[30] R. Storn, K. Price, Differential evolution–a simple and efficient heuristic for global optimization over continuous spaces, Journal of global optimization 11 (4) (1997) 341–359.
[31] F. Samimi, M. Bayat, D. Karimipourfard, M.R. Rahimpour, P. Keshavarz, A novel axial-flow spherical packed-bed membrane reactor for dimethyl ether synthesis: simulation and optimization, Journal of Natural Gas Science and Engineering 13 (2013) 42–51.
[32] F. Samimi, S. Kabiri, A. Mirvakili, M.R. Rahimpour, Simultaneous dimethyl ether synthesis and decalin dehydrogenation in an optimized thermally coupled dual membrane reactor, Journal of Natural Gas Science and Engineering 14 (2013) 77–90.
[33] F. Samimi, S. Kabiri, A. Mirvakili, M.R. Rahimpour, The concept of integrated thermally double coupled reactor for simultaneous production of methanol, hydrogen and gasoline via differential evolution method, Journal of Natural Gas Science and Engineering 14 (2013) 144–157.
[34] A. Mirvakili, F. Samimi, A. Jahanmiri, Optimization of Ammonium Nitrate Thermal Decomposition in a Fluidized Bed Reactor Using Differential Evolution (DE) Method, Chemical Engineering Communications 202 (5) (2015) 557–568.
[35] F. Samimi, M. Bayat, M.R. Rahimpour, P. Keshavarz, Mathematical modeling and optimization of DME synthesis in two spherical reactors connected in series, Journal of Natural Gas Science and Engineering 17 (2014) 33–41.
[36] F. Samimi, S. Kabiri, M.R. Rahimpour, The optimal operating conditions of a thermally double coupled, dual membrane reactor for simultaneous methanol synthesis, methanol dehydration and methyl cyclohexane dehydrogenation, Journal of Natural Gas Science and Engineering 19 (2014) 175–189.
[37] F. Samimi, A. Ahmadi, O. Dehghani, M.R. Rahimpour, DE Approach in Development of a Detailed Reaction Network for Liquid Phase Selective Hydrogenation of Methylacetylene and Propadiene in a Trickle Bed Reactor, Industrial & Engineering Chemistry Research 54 (1) (2014) 117–129.
[38] D. Karimipourfard, N. Nemati, M. Bayat, F. Samimi, M.R. Rahimpour, Mathematical Modeling and Optimization of Syngas Production Process: A Novel Axial Flow Spherical Packed Bed Tri-Reformer, Chemical Product and Process Modeling (2018).